DOI: 10.13009/EUCASS2019-719

DOI: ADD DOINUMBER HERE

A Comparative Study of the Aging Behavior of Different Nano-sized Aluminum Powders

Alberto Verga[⋆†] *and Christian Paravan*[⋆]
[⋆]*Politecnico di Milano, Department of Aerospace Science and Technology,*
Space Propulsion Laboratory (SPLab),
34 Via La Masa, 20156, Milan, Italy
alberto.verga@polimi.it · christian.paravan@polimi.it
[†]Corresponding author

Abstract

This paper studies the aging behavior of four nano-sized aluminum powders, stored under different conditions in terms of temperature and relative humidity. The nominal particle size of the powders is in the range 40 −200 nm. The particle size distribution of the fresh powders was assessed, as well as the particles morphology and structure, the composition and the reactivity.
The aging tests were carried out for periods of time that span from less than 24 hours to 6 months, depending on the storage conditions. The metal content and the low-heating rate reactivity of the aged powders were determined.

1. Introduction

In energetic applications, such as propellants, explosives and pyrotechnics, metals are widely employed thanks to the high combustion enthalpy and high energy density [1]. Focusing on rocket propulsion, the aim of adding metals to solid propellant formulation is to increase the flame temperature (i.e., the specific impulse) [2]. Among the available metals, aluminum is usually selected due to the good stability and low toxicity. Elements like beryllium feature higher enthalpy release during combustion, but their inherent drawbacks are the high toxicity of the reaction products and the pyrophoricity. In the field of solid propulsion, micron-sized aluminum powders have been successfully exploited. They are effective at increasing the specific impulse and damping the high-frequency pressure instabilities in the combustion chamber of solid rocket motors. The main drawback is the generation of condensed combustion products, that in turn leads to specific impulse losses due to the expansion of a two-phase flow through the gasdynamic nozzle [3]. For this reason, a trade-off fraction of micrometric aluminum in the range from 14 to 20 wt.% is usually loaded in metallized solid propellants. The partial substitution with nano-sized aluminum (nAl) grants higher steady burning rates and reduces the size of the combustion products. This is mainly due to the high reactivity of nano-sized powders, linked to the large specific surface area of the particles. However, this feature makes nAl powders more prone to react with water vapor if stored in a hot and humid environment [4]. In this regard, the Space Propulsion Laboratory (SPLab) of Politecnico di Milano is active in the pre-burning and aging characterization of micron- and nano-sized aluminum powders [5] [6].

2. Powders Characterization

In this work, four nano-sized aluminum powders were analyzed. A pre-aging characterization of the fresh powders was performed. The powders were produced by electric explosion of wires (EEW) and passivated by dry air right after the production, to stabilize the particles surface. Thus, aluminum particles produced by EEW are characterized by a metal core surrounded by a protective amorphous aluminum oxide layer. The EEW technique allows the production of powders with a particle size in the range 0.01 −1 µm [7]. Information on the nomenclature and the nominal particle size of the tested powders are given in Table 1.

The particle size distribution of n100 and n200 powders was evaluated by Malvern Mastersizer 2000. The two powders with a nominal size of 40 nm were not tested, because this value is below the sensitivity threshold of the analyzer. The powders were dispersed in ethanol to perform the measurement with the Hydro wet unit. The volume-

DOI: 10.13009/EUCASS2019-719

Table 1: General information on the tested *Al* powders.

Powder ID	**Nominal Particle Size,** nm	**Producer/Supplier**
n40c	40	Hongwu International Group, LTD
n40us	40	US Research Nanomaterials, Inc.
n100	100	APT, LLC/Fraunhofer ICT
n200	200	Hongwu International Group, LTD

weighted (D_{43}) and the surface-weighted mean diameter (D_{32}) were determined according to Equation 1, under the hypothesis of spherical particles [8]:

$$D_{43} = \frac{\sum_{i=1}^{n} D_i^4}{\sum_{i=1}^{n} D_i^3} \qquad D_{32} = \frac{\sum_{i=1}^{n} D_i^3}{\sum_{i=1}^{n} D_i^2} \tag{1}$$

The computed values are listed in Table 2. It can be noticed that n200 powder exhibits a D_{43} significantly higher than the nominal particle size. This is probably due to the presence of a coarse fraction in the powder, as evidenced by the SEM image presented in Figure 2(b). In fact, the volume-weighted mean diameter is more sensitive than D_{32} to the presence of large particles in the powder. Assuming spherical elements, the mean particle diameter (a_S) and the thickness of the alumina shell ($\delta_{Al_2O_3}$) of the tested powders were estimated as:

$$a_s = \frac{6}{\rho_{Al} \cdot SSA} \tag{2}$$

$$\delta_{Al_2O_3} = \frac{a_s}{2} - \left[\frac{\rho_{Al_2O_3} \cdot C_{Al} \cdot (a_s/2)^3}{\rho_{Al_2O_3} \cdot C_{Al} + \rho_{Al} \cdot (1 - C_{Al})} \right]^{1/3} \tag{3}$$

The results are shown in Table 2. The densities of aluminum ($\rho_{Al} = 2700\,\mathrm{kg/m^3}$) and its amorphous oxide ($\rho_{Al_2O_3} = 3050\,\mathrm{kg/m^3}$) were employed to perform the calculation. The specific surface area (SSA) of the fresh powders was determined by a sorption technique. The aluminum particles underwent physical adsorption of N_2 at 77 K. The BET model was then applied to the obtained data. The active aluminum content (C_{Al}) was evaluated by a volumetric method [9]. Small samples of each powder were placed in an acqueous solution of sodium hydroxide ($NaOH$) (5 wt.%). The obtained specific surface and C_{Al} values are presented in Table 2. It can be seen that, with the exception of n200, powders with a larger SSA show a lower metal content. This is due to the fact that *Al* particles with different sizes are surrounded by an Al_2O_3 layer of the same thickness [7]. Among the tested powders, n200 exhibits the smallest SSA and the lowest C_{Al}. The aluminum content reduction can be ascribed to the presence of a fine fraction with a size that is half the nominal particle diameter.

Table 2: Physical characterization of the tested *Al* powders.

Powder ID	D_{43}, nm	D_{32}, nm	a_s, nm	$\delta_{Al_2O_3}$, nm	SSA, $\mathrm{m^2/g}$	C_{Al}, wt.%
n40c	– [a]	– [a]	40.0 [b]	1.8	–	72.5 ± 1.5 [d]
n40us	– [a]	– [a]	90.7	3.6	24.5 ± 0.1 [c]	76.0 ± 1.4 [d]
n100	138	133	176.4	4.0	12.6 ± 0.1 [c]	85.5 ± 1.2 [d]
n200	560	261	261.4	13.8	8.5 ± 0.1 [c]	69.0 ± 1.4 [d]

[a] Lower than Malvern Mastersizer 2000 threshold.
[b] Nominal value.
[c] Systematic error of the experimental apparatus.
[d] Data scattering evaluated by standard deviation.

The morphology and structure of the aluminum particles were studied by means of electron microscopy techniques. Scanning electron microscopy (SEM) images exhibit the high clustering tendency typical of nano-sized powders, as shown in Figure 1(a) for n40us powder. Spherical particles and some necked elements can be identified. On the contrary, n40c exhibits prism-shaped particles with sharp edges (see Figure 1(b)) and a slightly lower metal content. This is due to the presence of a crystalline $AlO(OH)$ phase (4.6 wt.%), according to the X-ray diffraction (XRD) results. The Al_2O_3 shell hydration probably took place due to the exposition to air humidity during the powders production

DOI: 10.13009/EUCASS2019-719

or storage. SEM images of n100 powder show spherical and spheroid particles with a relatively smooth surface texture and a strong clustering behavior (see Figure 2(a)). Finally, both spherical and prismatic elements with a size less than 100 nm were identified for n200 powder, due to the 10.1 wt.% $AlO(OH)$ content. Micron-sized granules are also present, as evidenced in Figure 2(b).

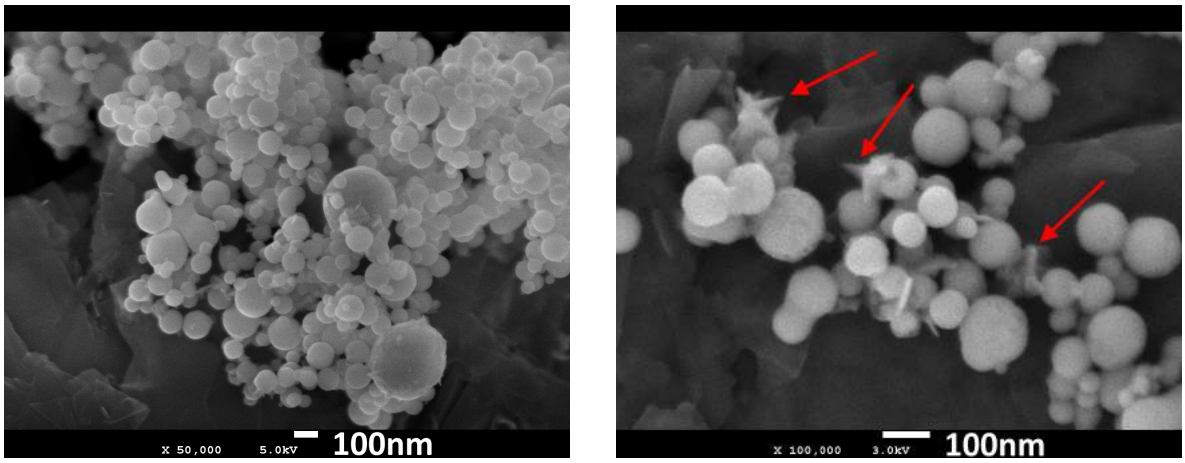

(a) (b)

Figure 1: SEM images of n40 powders: (a) groups of clustered particles with necked elements (n40us), (b) prism-shaped elements with sharp edges (n40c), see red arrows.

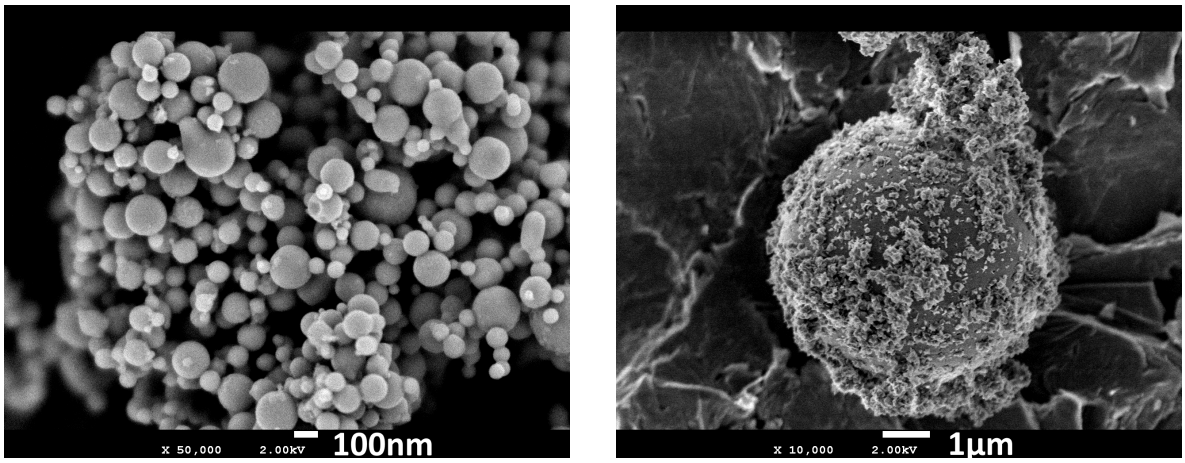

(a) (b)

Figure 2: SEM images of n100 and n200 powders: (a) groups of spherical particles with a relatively smooth surface (n100), (b) spherical and prism-shaped elements on a micron-sized granule (n200).

Transmission electron microscopy (TEM) images allowed the investigation of the structure of the aluminum particles. In particular, the typical Al core-Al_2O_3 shell structure was evidenced (see Figure 3(a)). The alumina layer thickness was measured, finding values in good agreement with those available in open literature (5 −7 nm) [10]. As shown in Figure 3(b), the necked particles seem to be surrounded by the same alumina shell.

To compare the reactivity of the tested powders, non-isothermal oxidation tests were performed in air. A Seiko EXSTAR 6000 simultaneous termogravimetric-differential thermal analyzer (TG-DTA) was employed. A 150 ml/min air flow and a low heating rate (10 K/min) were selected. Powder samples were heated up from 300 to 1300 K. The reactivity parameters were evaluated according to Ilyin et al. [11]. The computed values are listed in Table 3. As shown in Figure 4, the fresh powders show a mass loss (Δm_0) at relatively low temperature, due to the desorption of the gases adsorbed on the particles surface. Open literature studies underline the link between the powder specific surface area and Δm_0: the higher the SSA, the larger the initial mass loss. In this work, n200 powder represents the only exception to this trend (see Table 3). In fact, the significant mass loss under 700 K is probably linked to the aluminum

DOI: 10.13009/EUCASS2019-719

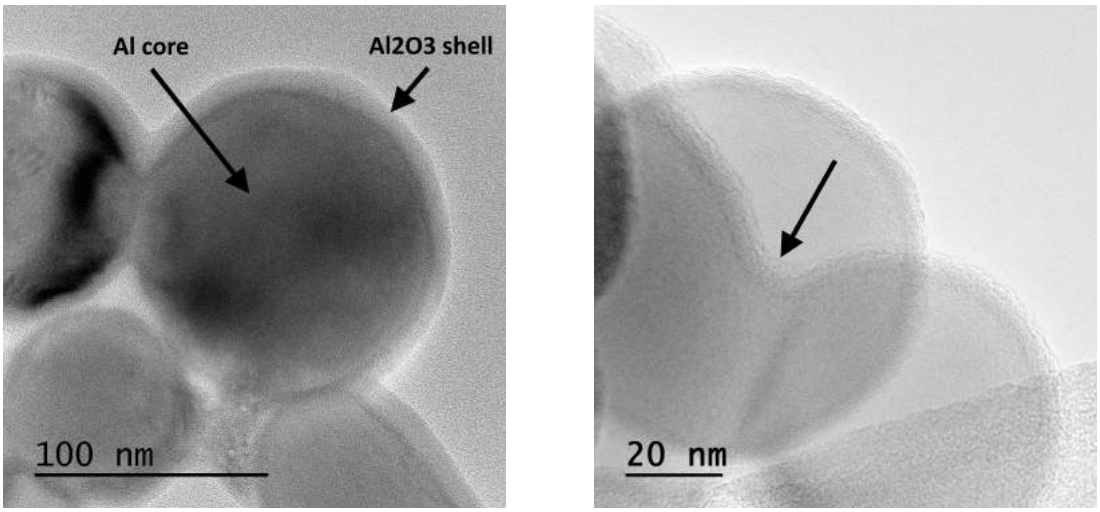

(a) (b)

Figure 3: TEM images of n40c and n100 powders: (a) typical Al core-Al_2O_3 shell structure (n40c), (b) necked particles that share the same alumina shell (n100), see black arrow.

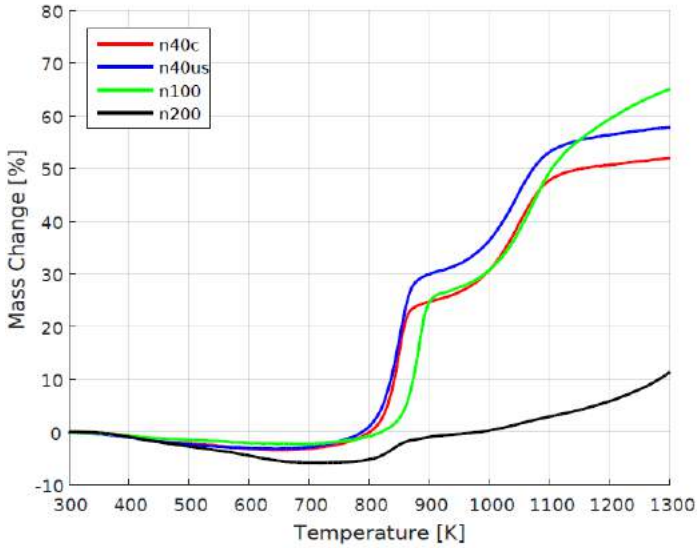

Figure 4: TG traces of the fresh powders (0.1 MPa, 150 ml/min air flow, 10 K/min heating rate).

hydroxide dehydration process [12]. The onset temperature of the first oxidation step ($T_{on,1}$) was determined by the Piloyan's method. The onset temperature due to non-isothermal oxidation in air is inversely proportional to the powder SSA (i.e., powder reactivity) [13]. Among the considered powders, n200 has the smallest specific surface area and the lowest onset temperature. In fact, the evaluation of the latter parameter was influenced by the mild slope of the first oxidation stage. This is due to the presence of the fine particulate shown in Figure 2(b), which probably begins to react at temperatures lower than the coarser fraction. The conversion factor of aluminum into its oxide ($\alpha_{Al\rightarrow Al_2O_3}(T)$) was evaluated at the Al melting temperature (933 K) as:

$$\alpha_{Al\rightarrow Al_2O_3}(T) = \frac{\Delta m(T)}{C_{Al} \cdot 0.89} \tag{4}$$

To perform the calculation, the mass gain at the reference temperature (Δm(933 K)) and the C_{Al} of the fresh powders were employed. The stoichiometric oxidation reaction between Al and gaseous oxygen was considered. As expected, the parameter monotonically increases with the powder reactivity (see Table 3).

DOI: 10.13009/EUCASS2019-719

Table 3: Reactivity parameters of the fresh *Al* powders.

Parameter	n40c	n40us	n100	n200
$T_{on,1}$, K	825.5 ± 1.3	820.9 ± 6.8	857.7 ± 1.6	807.9 ± 1.9
Δm_0, %	-3.1 ± 0.4	-2.5 ± 0.5	-2.1 ± 1.5	-6.1 ± 0.4
Δm(933 K), %	30.4 ± 1.1	33.9 ± 1.9	29.7 ± 1.4	5.1 ± 0.7
$\alpha_{Al\rightarrow Al_2O_3}$(933 K), %	47.1 ± 2.6	50.1 ± 3.3	38.8 ± 3.8	8.2 ± 2.0
Data scattering evaluated by standard deviation.				

3. Experimental Procedure and Results Discussion

In order to evaluate the aging behavior of the considered nano-sized aluminum powders, experiments under controlled storage conditions were performed. Sealed glass vessels were employed as containers. To set the relative humidity (RH) of the storage environment, each vessel was partially filled with an acqueous supersaturated salt solution [14]. To ensure a suitable RH value, sodium chloride ($NaCl$) was selected as salt. Finally, the powder samples were inserted in the containers, that in turn were closed and placed into a fan oven. The temperature inside the oven was controlled by means of a thermostat. Due to the interaction with humid air, aluminum was converted into bayerite ($Al(OH)_3$), thus changing the powder characteristics. The mass and C_{Al} of the powder samples were recorded before and after the storage period. Based on the sample mass variation in time ($\Delta m(t)$) due to aging, the degree of conversion of aluminum into its hydroxide ($\alpha_{Al\rightarrow Al(OH)_3}(t)$) was calculated as:

$$\alpha_{Al\rightarrow Al(OH)_3}(t) = \frac{\Delta m(t)}{C_{Al} \cdot 1.89} \tag{5}$$

In Equation 5, the C_{Al} value for the fresh powders and the maximum mass increase (i.e., 189%) due to the stoichiometric reaction between *Al* and water were considered. The four aluminum powders were stored at 333 K and 75% RH. As an example, the aging behavior of n40c under such conditions is shown in Figure 5. Three stages in the $Al \rightarrow Al(OH)_3$ transformation trend were identified. After an initial region of limited conversion, the process significantly speeds up, leading to a considerable sample mass gain. It can be noticed that this fast-reaction region is characterized by a high data scattering. Then, the conversion rate slows down until the nearly complete C_{Al} consumption. The same three-steps mechanism is exhibited by the active aluminum content reduction in time. For the n200 powder a 30 wt.% of C_{Al} is left at the end of a 96 hours storage period. This might be linked to the previously discussed presence of a micron-sized fraction in the powder.

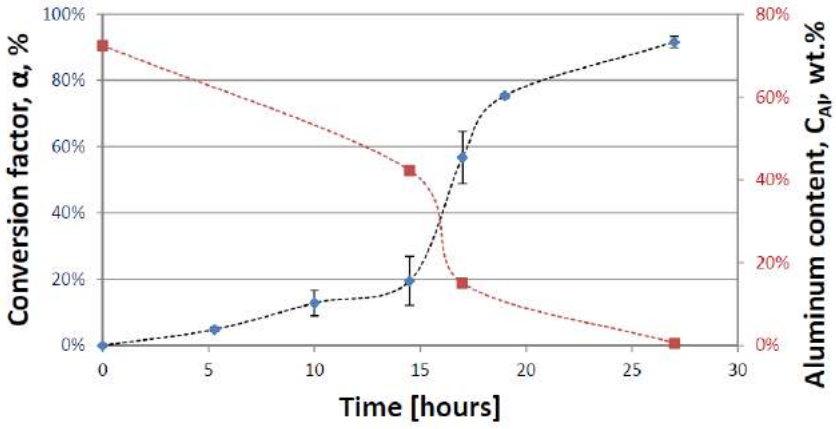

Figure 5: Degree of conversion $\alpha_{Al\rightarrow Al(OH)_3}(t)$ and C_{Al} of n40c during short-term storage (333 K, 75% RH). Interpolating curves are plotted for readability purposes.

The reactivity of the aged powders was evaluated by TG-DTA analysis. Samples at $\alpha_{Al\rightarrow Al(OH)_3}(t)$ in the range 40-45% were considered. To compare the reactivity parameters to those of the fresh *Al* powders, non-isothermal oxidation tests were performed under the same conditions (i.e., 150 ml/min air flow, 10 K/min heating rate). A selection of the data obtained for n40us and n100 powders is reported in Table 4. The faint diminution of the onset temperature $T_{on,1}$

DOI: 10.13009/EUCASS2019-719

is caused by the slope decrease of the first oxidation step, that hinders the correct evaluation of the parameter. It can be noticed an increase of the mass loss Δm_0 with respect to the fresh powders. This is due to the dehydration of the bayerite generated during storage by the reaction between *Al* and the humid environment [12]. On the contrary, the aged powders show a reduced $\alpha_{Al\rightarrow Al_2O_3}(933\,\mathrm{K})$ conversion factor. In fact, the increase of the alumina layer thickness acts as a barrier against the humid air diffusion towards the *Al* core.

Table 4: Reactivity parameters of the aged n40us and n100 powders.

Parameter	n40us		n100	
	Fresh	Aged	Fresh	Aged
$T_{on,1}$, K	820.9 ± 6.8	811.5 ± 0.6	857.7 ± 1.6	849.3 ± 1.1
Δm_0, %	-2.5 ± 0.5	-20.5 ± 1.0	-2.1 ± 1.5	-23.2 ± 0.1
Δm(933 K), %	33.9 ± 1.9	10.6 ± 1.5	29.7 ± 1.4	7.1 ± 0.2
$\alpha_{Al\rightarrow Al_2O_3}$(933 K), %	50.1 ± 3.3	27.9 ± 2.9	38.8 ± 3.8	16.0 ± 2.6
Data scattering evaluated by standard deviation.				

To investigate the effect of temperature on the aging behavior of nano-sized aluminum powders [6], n100 was stored for 6 months at 298 K without changing the relative humidity level with respect to the short-term experimental campaign. As shown in Figure 6, the Al_2O_3 shell that surrounds the aluminum particles exhibits a protective action on the metal core, preventing it from reacting with the humid environment. During the whole storage period, less than 2 wt.% of the fresh powder C_{Al} was converted into aluminum hydroxide.

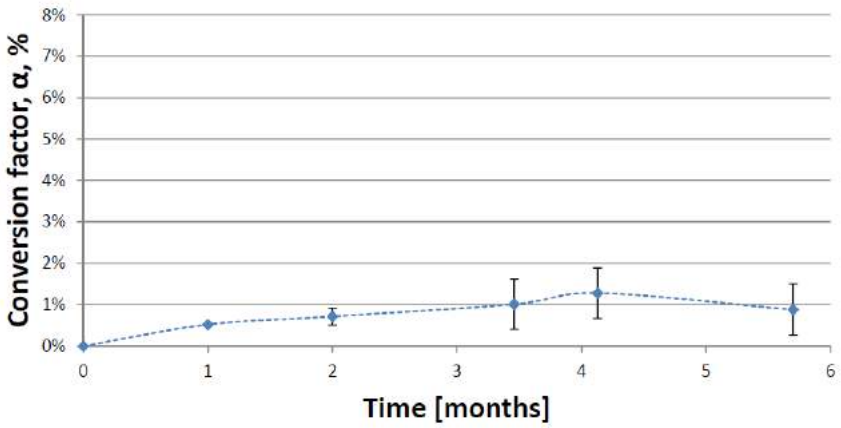

Figure 6: Degree of conversion $\alpha_{Al\rightarrow Al(OH)_3}(t)$ of n100 during long-term storage (298 K, 75% RH). Interpolating curve is plotted for readability purposes.

4. Conclusions

The aging behavior of four nano-sized aluminum powders with a nominal particle size in the range 40 −200 nm was investigated. A thermophysical characterization of the fresh powders was carried out. The composition was determined by XRD analysis. For all the powders, aluminum was detected as crystalline phase, while a $AlO(OH)$ fraction was identified in n40c and n200 samples (4.6 and 10.1 wt.%, respectively). The active aluminum content was evaluated by a volumetric method. Despite the large particle size, n200 exhibited the lowest C_{Al} among the tested powders. This is due to the considerable hydroxide content and to the presence of a finer particulate in the powder, as observed by SEM images. Scanning electron microscopy allowed the study of the particles morphology. The high-clustering tendency typical of nano-sized powder was evidenced. Spherical particles with a smooth surface were identified, together with prism-shaped elements in the case of n40c and n200 samples. Particles analyzed by transmission electron microscopy exhibited the peculiar *Al* core-Al_2O_3 shell structure. An alumina layer thickness of 5.5 nm was obtained from TEM images. Being amorphous, Al_2O_3 was not detected by XRD. The reactivity was determined by non-isothermal oxidation in air at low heating rate (10 K/min). As shown by the calculated reactivity parameters, a reduction of the particle size leads to an increase of the powder reactivity. All the investigated powders were stored under controlled conditions in

DOI: 10.13009/EUCASS2019-719

terms of temperature and relative humidity (333 K, 75% RH). Sample mass and C_{Al} were monitored in time during the storage. A three-steps aging mechanism was identified. After an initial induction period, all the powders exhibited a region of fast reaction between *Al* and the humid environment, followed by a slowdown of the process until the complete C_{Al} consumption. Depending on the particle size, the complete conversion of aluminum into $Al(OH)_3$ took from 1 to 4 days. On the contrary, 30 wt.% of the aluminum content of n200 samples remained unreacted after more than 96 hours of storage, due to the presence of a micron-sized fraction in the powder. The parameters evaluated by TG-DTA analysis suggested a reduction of the powder reactivity due to storage in a hot and humid environment. The effect of temperature on the aging behavior of n100 powder was studied. At 298 K and 75% RH, no significant variations in the powder C_{Al} and reactivity could be identified within a storage period of 6 months.

5. Future Developments

The obtained results suggest to consider the following points as future work development:

- evaluation of low and intermediate relative humidity levels to better assess the influence of this parameter for storage conditions at industrial level;
- determination of the effects of powders transformation (in terms of size, morphology, composition and reactivity) due to aging on solid propellants performances;
- implementation of a mathematical model for the description of the alumina shell hydration, that in turns leads to humid air diffusion towards the aluminum particle core. The hydroxide content of the fresh powder should be taken into account as a governing factor.

Acknowledgments

Authors thank Alessio Alo' for the valuable experimental activity, and Dr. Gianluigi Marra (Renewable Energies and Environment R & D, Istituto ENI Donegani, Novara, Italy) for XRD, SEM, and TEM data and helpful discussions.

References

[1] E. L. Dreizin. "Metal-Based Reactive Nanomaterials". In: *Progress in Energy and Combustion Science* 35.2 (2009), pp. 141–167.

[2] L. T. De Luca et al. "Characterization and Combustion of Aluminum Nanopowders in Energetic Systems". In: *Metal Nanopowders: Production, Characterization, and Energetic Applications*. Ed. by A. A. Gromov and U. Teipel. Wiley-VCH, 2014. Chap. 12, pp. 301–410.

[3] V. A. Babuk, V. A. Vasilyev, and M. S. Malakhov. "Condensed Combustion Products at the Burning Surface of Aluminized Solid Propellant". In: *Journal of Propulsion and Power* 15.6 (1999), pp. 783–793.

[4] M. Cliff, F. Tepper, and V. Lisetsky. "Ageing Characteristics of ALEX Nanosize Aluminum". In: *37th AIAA/ASME/SAE/ASEE Joint Propulsion Conference and Exhibit*. July 2001, p. 3287.

[5] C. Paravan et al. "Aging Effects on Nano-Sized Aluminum Reactivity". In: *7th European Conference for Aerospace Sciences (EUCASS)*. July 2017, pp. 1–14.

[6] C. Paravan et al. "Accelerated Ageing of Micron- and Nano-Sized Aluminum Powders: Metal Content, Composition and Non-Isothermal Oxidation Reactivity". In: *Acta Astronautica* 158 (2019), pp. 397–406.

[7] Y. F. Ivanov et al. "Productions of Ultra-Fine Powders and Their Use in High Energetic Compositions". In: *Propellants, Explosives, Pyrotechnics* 28.6 (2003), pp. 319–333.

[8] A. Rawle. "Basic Principles of Particle Size Analysis". In: *Surface Coatings International* 86.2 (2003), pp. 58–65.

[9] L. Chen et al. "Research on the Methods to Determine Metallic Aluminum Content in Aluminum Nanoparticles". In: *Materials Chemistry and Physics* 120.2 (2010), pp. 670–675.

[10] Y.-S. Kwon et al. "Passivation Process for Superfine Aluminum Powders Obtained by Electrical Explosion of Wires". In: *Applied Surface Science* 211.1 (2003), pp. 57–67.

[11] A. P. Ilyin et al. "Characterization of Aluminum Powders: I. Parameters of Reactivity of Aluminum Powders". In: *Propellants, Explosives, Pyrotechnics* 27.6 (2002), pp. 361–364.

DOI: 10.13009/EUCASS2019-719

[12] T. Sato. “Thermal Decomposition of Aluminium Hydroxides”. In: *Journal of Thermal Analysis and Calorimetry* 32.1 (1987), pp. 61–70.

[13] A. P. Ilyin, A. A. Gromov, and G. V. Yablunovskii. “Reactivity of Aluminum Powders”. In: *Combustion, Explosion, and Shock Waves* 37.4 (2001), pp. 418–422.

[14] S. Pisharath, F. Zhang, and H. G. Ang. “Influence of Passivation on Ageing of Nano-Aluminum: Heat Flux Calorimetry and Microstructural Studies”. In: *Thermochimica Acta* 635 (2016), pp. 59–69.